The Predictive Power of Computational Astrophysics as a Discovery Tool
Proceedings IAU Symposium No. 362, 2023
D. Bisikalo, D. Wiebe & C. Boily, eds.
doi:10.1017/S1743921322001351

Mass ejection from neutron-star mergers

Masaru Shibata[1,2], Sho Fujibayashi[1], Kota Hayashi[2], Kenta Kiuchi[1,2] and Shinya Wanajo[1]

[1]Max Planck Institute for Gravitational Physics (Albert Einstein Institute), am Mühlenberg 1, Potsdam-Golm D-14476, Germany
email: mshibata@aei.mpg.de

[2]Center for Gravitational Physics, Yukawa Institute for Theoretical Physics, Kyoto University, Kyoto 606-8502, Japan

Abstract. Merger of binary neutron stars and black hole-neutron star binaries is the promising source of short-hard gamma-ray bursts, the most promising site for the r-process nucleosynthesis, and the source of kilonovae. To theoretically predict the merger and mass ejection processes and resulting electromagnetic emission, numerical simulation in full general relativity (numerical relativity) is the unique approach. We summarize our current understanding for the processes of neutron-star mergers and subsequent mass ejection based on the results of long-term numerical-relativity simulations. We pay particular attention to the electron fraction of the ejecta.

Keywords. Neutron-star merger, Kilonovae, Numerical Relativity, Nucleosynthesis

1. Introduction

Merger of neutron-star binaries (binary neutron stars (NS-NS) and black hole-neutron star (BH-NS) binaries) is one of the most promising sources of gravitational waves for ground-based advanced detectors, such as advanced LIGO and advanced Virgo (Abbott et al. 2021). These detectors have already observed gravitational waves from two NS-NS and three BH-NS binaries (Abbott et al. 2021), and thus, it is natural to expect that they will detect a number of gravitational-wave signals from NS binaries in the next decade.

In Shibata & Hotokezaka (2019), we summarized our understanding for the merger and mass ejection processes of NS binaries in 2018. Since then, several numerical simulations with all the relevant physical contents such as general relativity, neutrino cooling and heating, and magneto/viscous hydrodynamical angular momentum transport for a long timescale of 1–10 s have been performed for exploring the evolution of the post-merger systems, and as a result, our understanding has been deepened in the last three years. In particular, for the case that the merger remnant is a black hole, our understanding for the property of the post-merger ejecta has been updated. Thus, in this article we summarize our latest understanding for the ejecta paying particular attention to the update of our knowledge on the post-merger ejecta.

2. Merger remnants and their evolution

The fate of NS binaries depends on the mass (m_1, m_2) and spin of binary components, and the NS equation of state (EOS). For NS-NS binaries, for which the effect of their spin is minor, the total mass $(M_{\rm tot} = m_1 + m_2)$, the mass ratio $(q = m_2/m_1\ (\leqslant 1))$ of the system, and the EOS are the key quantities for determining the merger remnant. For BH-NS binaries, the BH spin as well as the mass ratio and the EOS are the keys.

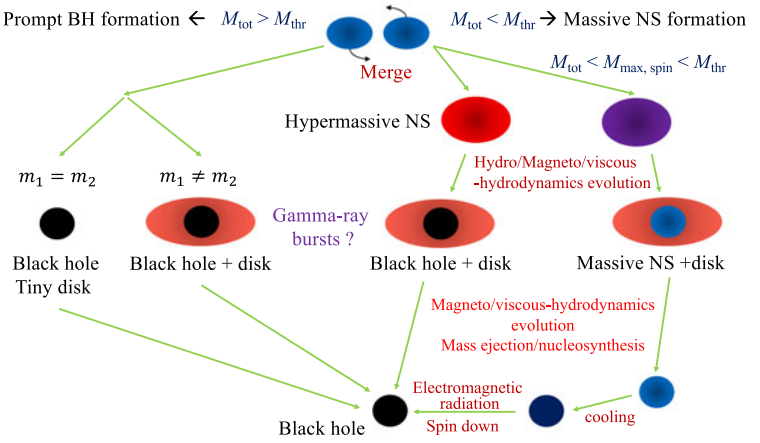

Figure 1. A summary for the merger and post-merger evolution of NS-NS binaries. $M_{\rm thr}$ and $M_{\rm max,spin}$ denote the threshold mass for the prompt formation of a BH and the maximum mass of rigidly rotating cold NSs, respectively. Their values are likely to be $M_{\rm thr} \gtrsim 2.8 M_\odot$ and $M_{\rm max,spin} \gtrsim 2.4 M_\odot$. For the total mass $M_{\rm tot} > M_{\rm thr}$, a BH is formed in the dynamical timescale after the onset of merger, and for the nearly equal-mass case, $m_1 \approx m_2$, the mass of disks surrounding the BH is tiny $\ll 10^{-2} M_\odot$, while it could be $\gtrsim 10^{-2} M_\odot$ for a highly asymmetric system with $m_2/m_1 \lesssim 0.8$. For $M_{\rm max,spin} < M_{\rm tot} < M_{\rm thr}$, a *hypermassive* neutron star (HMNS) is formed, and it subsequently evolves through several angular-momentum transport/dissipation processes, leading to eventual collapse to a BH surrounded by a disk (or torus). See, e.g., Shibata 2016 for the definition of the HMNS (and SMNS referred to below). For the case that $M_{\rm tot}$ is close to $M_{\rm thr}$, the lifetime of the MNS is relatively short, while for smaller values of $M_{\rm tot}$ toward $M_{\rm max,spin}$, the lifetime is longer. For the longer lifetime, the angular-momentum transport process works for a longer timescale, and the disk mass could be $\gtrsim 0.1 M_\odot$, whereas for a short lifetime, it could be $\sim 10^{-2} M_\odot$ or less. For $M_{\rm tot} < M_{\rm max,spin}$, a *supramassive* neutron star (SMNS) is formed and it will be alive for a dissipation timescale of its angular momentum which will be much longer than the neutrino cooling timescale of 1–10 s. Note that MNS denotes either an SMNS or an HMNS.

Figure 1 summarizes the possible remnants and their evolution processes for NS-NS mergers. Broadly speaking, there are two possible remnants formed immediately after the onset of merger; a BH and a massive neutron star (MNS). A BH is formed if the total mass ($M_{\rm tot}$) is so high that the self gravity of the merger remnant cannot be sustained by the pressure associated primarily with the repulsive force among nucleons and centrifugal force due to rapid rotation resulting from the orbital angular momentum of the pre-merger binary. An important finding for many numerical-relativity simulations performed in the last two decades is that for $M_{\rm tot} \lesssim 2.8 M_\odot$, the remnant is, at least temporarily, an MNS not a BH irrespective of the EOS that can reproduce $\gtrsim 2 M_\odot$ NSs. The total mass of NS-NS for GW170817 is $2.74^{+0.04}_{-0.01} M_\odot$ for a reasonable low spin prior (Abbott et al. 2017), and thus, for this event, an MNS is likely to be formed at least temporarily. By contrast, for GW190425 (Abbott et al. 2020) for which the total mass is $\sim 3.4 M_\odot$, a BH is likely to be formed immediately after the onset of the merger.

For the case of the prompt formation of a BH in NS-NS mergers, the dimensionless BH spin, χ, is approximately 0.8. The remnant BH in this formation channel is not surrounded by a massive disk if the mass ratio q is close to unity. The mass of the remnant disk around the BH increases with the decrease of q, and in the presence of a significant mass asymmetry, $q \lesssim 0.8$, the disk mass could be $\gtrsim 10^{-2} M_\odot$ (cf. Fig. 1). The disk around the BH is likely to be evolved by magnetohydrodynamics (MHD) processes, in particular by the effect of MHD turbulence induced by magnetorotational

https://doi.org/10.1017/S1743921322001351 Published online by Cambridge University Press

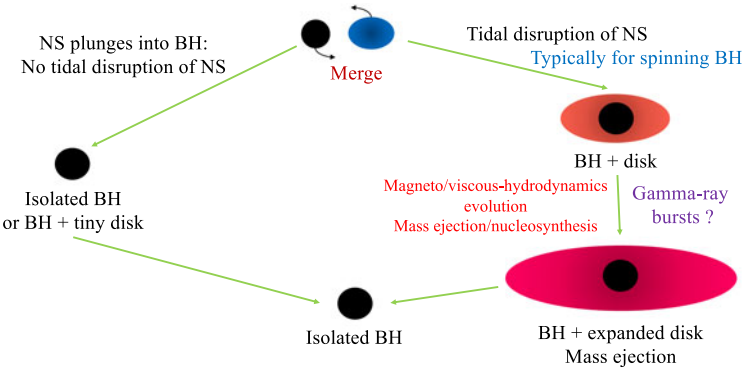

Figure 2. Two possible fates for the merger and post-merger evolution of BH-NS binaries; the NS is tidally disrupted (right path) or not (left path) by the companion BH. The tidal disruption is more subject for a spinning BH with the spin aligned with the orbital angular momentum. For the presence of tidal disruption, thus, the remnant is typically a rapidly spinning BH surrounded by a disk. The evolution process of the BH-disk system is essentially the same as that for NS-NS mergers.

instability (MRI) (Balbus & Hawley 1998) and winding, and resultant turbulent viscous process. During the MHD and viscous evolution of the disk, a short gamma-ray burst (sGRB) could be launched by the Blandford-Znajek mechanism (Blandford & Znajek 1977) associated with the strong magnetic field generated by the MHD turbulence which subsequently forms a BH magnetosphere. The viscous effect in the disk plays a central role for the post-merger mass ejection (see § 3.2).

For BH-NS binaries for which the NS is tidally disrupted at a close orbit, the remnant is also a BH surrounded by a disk. However, the disk mass can have a variety for this system. If the tidal disruption takes place far from the innermost stable circular orbit of the BH, the disk mass can be far beyond $10^{-2}M_\odot$. This is the case if the original BH is spinning rapidly and the spin is aligned with the orbital angular momentum (Kyutoku et al. 2021). Also in the presence of the tidal disruption of the NS, the remnant BH should be rapidly rotating as in the original BH, and thus, an sGRB associated with the Blandford-Znajek effect is also promising. For BH-NS binaries of low BH spin or of the high BH mass (say much larger than $10M_\odot$), the tidal disruption of the NS is unlikely to take place. In such cases, no or tiny mass of the disk and ejecta is expected (cf. Fig. 2).

For the MNS formation from NS-NS mergers, its evolution is determined by several processes. Soon after its formation, the gravitational torque associated with non-axisymmetric structure of the merger remnant plays an important role for transporting angular momentum from the MNS to matter surrounding it. This process reduces the angular momentum of the MNS while developing the disk formation. In addition, the MNS emits gravitational waves, and dissipates energy and angular momentum. Thus, if it is marginally stable against gravitational collapse, the MNS can collapse to a BH in ~ 100 ms by the angular momentum transport/dissipation. Numerical-relativity simulations have shown that the resulting system is a spinning BH of $\chi \sim 0.6$–0.7 surrounded by a disk of mass 10^{-2}–$10^{-1}M_\odot$ (see the references in Shibata & Hotokezaka (2019)). The disk mass is larger for the longer lifetime of the MNS and for more asymmetric systems of $q < 1$.

If the lifetime of the MNS is longer than ~ 100 ms, angular-momentum transport effects resulting from MHD turbulence are likely to play a role for the evolution of the MNS. At its formation, the MNS is differentially rotating. Furthermore, it should be strongly magnetized and in an MHD turbulence state with an excited turbulent

https://doi.org/10.1017/S1743921322001351 Published online by Cambridge University Press

viscosity, because at merger, a shear layer is formed at the contact surfaces of two NSs and the Kelvin-Helmholtz instability intensively occurs (Price & Rosswog 2006; Kiuchi et al. 2014). By this instability, a number of small-size vortexes are generated in the shear layer and magnetic fields are wound up by the vortex motion, which enhances the magnetic-field strength in a timescale much shorter than the dynamical timescale of the system ~ 0.1 ms. Note that the growth timescale of the Kelvin-Helmholtz instability is $\tau_{\rm KH} \sim 10^{-7}(\lambda/1\,{\rm cm})$ ms for the wavelength λ because the typically velocity at the onset of merger is $\sim 10^{10}$ cm/s. Because of the presence of the differential rotation and turbulent viscosity, the angular momentum in the MNS should be transported outward, and as a result, the inner part of the MNS is likely to settle to a nearly rigidly rotating state (e.g., Shibata et al. 2021). Simultaneously, a massive disk surrounding the MNS is developed because of the outward angular momentum transport in the outer region of the MNS. During the turbulent evolution in the MNS, the magnetic-field strength may be further amplified by the dynamo action. If global magnetic fields are generated during the dynamo action, the magnetic braking can also play a role for transporting the angular momentum of the MNS to the matter surrounding it.

If the lifetime of the MNS is even longer (i.e. MNS mass is not very large), it could be evolved by the viscous angular momentum transport to the disk from the contact region with the MNS and cooling by neutrino emission. The viscous timescale is approximately written as

$$\tau_{\rm vis,disk} \approx 0.2\,{\rm s} \left(\frac{\alpha_{\rm vis}}{10^{-2}}\right)^{-1} \left(\frac{c_s}{c/10}\right)^{-1} \left(\frac{R_{\rm inn}}{20\,{\rm km}}\right) \left(\frac{H/R_{\rm inn}}{1/3}\right)^{-1}, \tag{2.1}$$

where $\alpha_{\rm vis}$, c_s, $R_{\rm inn}$, and H are the dimensionless viscous parameter, the sound speed, the inner disk radius, and scale height there. The neutrino cooling timescale for MNSs is

$$\tau_\nu \approx \frac{U}{L_\nu} = 1\,{\rm s} \left(\frac{U}{10^{53}\,{\rm erg}}\right) \left(\frac{L_\nu}{10^{53}\,{\rm erg/s}}\right)^{-1}, \tag{2.2}$$

where U is total thermal energy of the MNS and L_ν is total neutrino luminosity. Note that at the formation of the MNS (including the disk and envelope region), $L_\nu \gtrsim 10^{53}$ erg/s, because shock heating at merger significantly increases its temperature, but in ~ 100 ms after its formation, L_ν deceases to $O(10^{52})$ erg/s (e.g., Fujibayashi et al. 2018). Thus, if the viscous angular momentum transport or the neutrino cooling has a significant effect and it is marginally stable to gravitational collapse, the MNS would collapse to a BH in either of these timescales.

If the MNS mass is low enough, it will not collapse to a BH in ~ 10 s, but the MNS is likely to settle to a rigidly rotating cold NS (the so-called SMNS). The maximum mass of the SMNS is by up to ~ 0.3–$0.4 M_\odot$ larger than the maximum mass of the non-spinning cold NS, $M_{\rm max}$ (Cook et al. 1994). Thus, if the value of $M_{\rm max}$ is, e.g., $2.1 M_\odot$, the maximum mass for SMNSs would be $M_{\rm max,spin} \sim 2.4$–$2.5 M_\odot$, and hence, the strong self gravity of the SMNS could be sustained. However, the SMNS is magnetized. Thus, its rotational kinetic energy is inevitably dissipated by the magnetic dipole radiation or magnetic braking effect. Assuming the presence of a dipole magnetic radiation with the luminosity $L_{\rm B}$, the spin-down timescale of the SMNS by the magnetic-dipole radiation is

$$\tau_B \approx \frac{T_{\rm rot}}{L_{\rm B}} \approx 9 \times 10^2\,{\rm s} \left(\frac{B_p}{10^{15}\,{\rm G}}\right)^{-2} \left(\frac{M_{\rm MNS}}{2.5 M_\odot}\right) \left(\frac{R}{15\,{\rm km}}\right)^{-4} \left(\frac{\Omega}{6000\,{\rm rad/s}}\right)^{-2}, \tag{2.3}$$

where $T_{\rm rot} (\sim 0.3 M_{\rm MNS} R^2 \Omega^2)$ is rotational kinetic energy, B_p the magnetic-field strength of the SMNS pole, and Ω the angular velocity of the SMNS. We assumed that the magnetic-field strength would be significantly enhanced at merger or during the dynamo action in the post-merger stage. This estimate shows that the rotational kinetic energy

https://doi.org/10.1017/S1743921322001351 Published online by Cambridge University Press

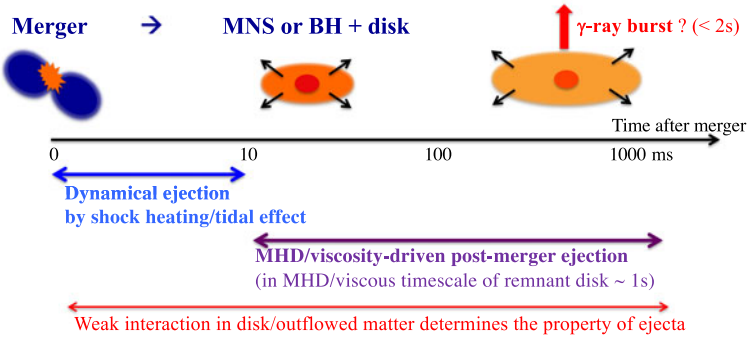

Figure 3. Mass ejection mechanisms during and after merger of NS binaries. Soon after the onset of merger, dynamical mass ejection takes place in the timescale of $\lesssim 10\,$ms. Subsequently, MHD- or viscosity-driven mass ejection occurs. In the post-merger evolution, the weak interaction process is the key for determining the electron fraction of the ejecta.

could be dissipated in $\sim 10^3\,$s. After the dissipation of its rotational kinetic energy, the SMNS should collapse to a BH.

3. Mass ejection

During the merger and post-merger evolution of merger remnants, neutron-rich matter is in general ejected. At the merger, the matter is dynamically ejected in the timescale of $\lesssim 10\,$ms. Such mass ejection is referred to as the dynamical mass ejection. Subsequently, the mass ejection can proceed from the merger remnant, in particular from the remnant disk, through MHD and viscous processes. Such mass ejection is referred to as the post-merger mass ejection (see Fig. 3 for these mass ejection processes). In the following, we summarize the mechanisms for these two mass ejections separately. We focus in particular on the mass, velocity, and electron fraction of the ejecta because these quantities determine the property of the nucleosynthesis and electromagnetic counterparts associated with the ejecta.

3.1. *Dynamical mass ejection*

At merger of NS-NS binaries, strong shock waves are generated because two NSs with high relative velocity $\gtrsim 0.3c$ collide. In the shock waves, kinetic energy associated with the plunging motion is converted to thermal energy, which enhances thermal pressure and induces the ejection of the shocked matter. Also, if an MNS is the merger remnant at least temporally, the resulting non-axisymmetric MNS gravitationally exerts torque to the matter in the outer region and induces quick angular-momentum transport. By this process, a fraction of the matter gains energy sufficient for being ejected from the system. These two mechanisms drive dynamical mass ejection for NS-NS mergers. For the BH-NS case, the dynamical mass ejection takes place when the NS is tidally disrupted. During the tidal disruption process, the NS is deformed in a non-axisymmetric shape, which induces the angular momentum transport and resulting mass ejection. Also, during the dynamical infall of the NS matter into the BH, the spacetime structure is modified; e.g., the quadrupole moment of the entire system is reduced. With this dynamical effect, the matter outside the BH receives a gravitational impact and the mass ejection is induced. The timescale of the dynamical mass ejection is $\lesssim 10\,$ms both for the NS-NS and BH-NS cases. By the tidal torque, matter is ejected primarily in the equatorial direction, while by shock heating, the matter is ejected in a quasi-isotropic manner.

https://doi.org/10.1017/S1743921322001351 Published online by Cambridge University Press

Mass: The mass of dynamical ejecta depends on the total mass, $M_{\rm tot}$, mass ratio, q, and NS compactness (i.e., EOS) for NS-NS binaries (e.g., Hotokezaka et al. 2013; Shibata et al. 2017; Radice et al. 2018; Nedora et al. 2021). For the BH-NS case, the mass ratio and the BH spin are key parameters (Kyutoku et al. 2021). As summarized in Fig. 1, for $M_{\rm tot} > M_{\rm thr}$, a BH is promptly formed after the onset of NS-NS mergers. For $q \approx 1$ with $M_{\rm tot} > M_{\rm thr}$, $\geq 99.9\%$ of the NS matter is swallowed into the formed BH, and appreciable mass ejection cannot take place. For asymmetric NS-NS mergers, a fraction of matter may be dynamically ejected even for $M_{\rm tot} > M_{\rm thr}$, and for this case, short-term shock heating and tidal torque exerted by a deformed merger object collapsing to a BH are the engines for the dynamical mass ejection. However, numerical-relativity simulations indicate that for the dynamical mass ejection with mass $\geqslant 10^{-3} M_\odot$ only for $q \lesssim 0.8$ (e.g., Hotokezaka et al. 2013).

For the MNS formation case from NS-NS mergers, the dynamical ejecta mass depends strongly on the compactness (i.e., EOS) of NSs as well as $M_{\rm tot}$. If the EOS is stiff (i.e., for a large NS radius), the relative velocity of two NSs at merger is relatively low, because the minimum orbital separation is relatively large, and thus, shock heating efficiency is relatively low. This results in small dynamical ejecta mass. Due to essentially the same reason, the dynamical ejecta mass depends on the total mass of the system, because for high total mass, shock heating efficiency can be high, resulting in large dynamical ejecta mass. Numerical-relativity simulations show that for EOSs with $R_{\rm NS} \gtrsim 13$ km or for $M_{\rm tot} \lesssim 2.6 M_\odot$, the dynamical ejecta mass is of $O(10^{-3}) M_\odot$ for $q \sim 1$. Even for $q \sim 0.8$, the dynamical ejecta mass could be at most $0.003 M_\odot$. On the other hand, for $R_{\rm NS} \lesssim 12$ km with $M_{\rm tot} \gtrsim 2.7 M_\odot$, the dynamical ejecta mass could be ~ 0.003–$0.01 M_\odot$ depending on q.

For BH-NS mergers, the mass of dynamical ejecta is determined by how tidal disruption of NSs proceeds. If an NS is tidally disrupted far from the innermost stable circular orbit around its companion BH, a large fraction of the NS matter (0.1–$0.3 M_\odot$) stays outside the BH horizon. This is in particular the case for rapidly spinning BHs. Numerical-relativity simulations show that for such a case, $\sim 10\%$–30% of the matter located outside the horizon can escape from the system as ejecta (for plausible BH mass of $\gtrsim 4 M_\odot$). Thus, larger disk mass results in larger dynamical ejecta mass, up to $\sim 0.1 M_\odot$ for the maximum case. By contrast, if NSs are not tidally disrupted, the dynamical ejecta mass (as well as the disk mass) is negligible. Thus, the dynamical ejecta mass is in a wide range of 0–$0.1 M_\odot$ for BH-NS mergers.

Velocity: Because the dynamical mass ejection proceeds near the last stable binary orbit of radius r, the velocity of the ejecta should be of the order of the escape velocity there, i.e., $\sim \sqrt{GM_{\rm tot}/r} \approx 0.33c (M_{\rm tot}/3M_\odot)^{1/2} (r/40\,{\rm km})^{-1/2}$. Numerical-relativity simulations have shown that the typical average velocity is indeed 0.15–$0.25c$ for the MNS formation case (e.g., Shibata & Hotokezaka 2019). For this case, the dynamical mass ejection is induced both by the shock heating and tidal torque. For the component ejected by the shock heating, a fraction of matter could have a relativistic speed up to $\sim 0.8c$ and, in addition, the ejecta morphology is quasi-spherical. For the prompt formation of a BH from highly asymmetric NS-NS binaries, the average velocity of ejecta can exceed $\sim 0.3c$, because the dynamical mass ejection proceeds only for the matter in the vicinity of the object collapsing to a BH by a tidal torque exerted.

For BH-NS mergers, the average velocity of the dynamical ejecta is 0.2–$0.3c$; it is higher for the rapidly spinning BHs with the spin axis aligned with the orbital angular momentum. By contrast to the MNS formation case of NS-NS mergers, the maximum velocity is always $\lesssim 0.4c$. The maximum velocity is higher for the rapidly spinning BHs.

https://doi.org/10.1017/S1743921322001351 Published online by Cambridge University Press

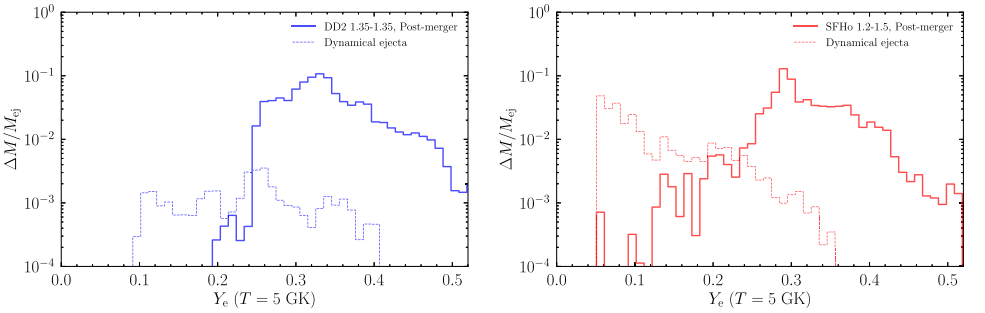

Figure 4. Mass histogram as a function of Y_e for the formation of a long-lived MNS (left) and a HMNS that collapses into a BH at ~ 20 ms after the onset of merger (right). The dotted and solid curves denote the contribution from dynamical and post-merger ejecta, respectively.

Electron fraction: The electron fraction (Y_e) of ejecta is one of the key quantities for determining elements synthesized by the r-process nucleosynthesis. Because the abundance pattern of the r-process elements is the key input for determining the opacity of the kilonova emission from the merger ejecta, the electron fraction is one of the most important quantities for determining the output after NS mergers (Barnes & Kasen (2013); Tanaka & Hotokezaka (2013)).

Because the typical value of Y_e for cold NSs is quite low, 0.01–0.1, Y_e of the dynamical ejecta would be also low if the NS matter is ejected without undergoing weak interaction processes. However, the property of the ejecta could be influenced strongly by the weak processes. First, shock heating at merger and during subsequent evolution of the merger remnant increases the matter temperature beyond 10 MeV in particular for NS-NS mergers. In such a high-temperature environment, the electron-positron pair creation is enhanced. Then, neutrons efficiently capture positrons via $n + e^+ \to p + \bar{\nu}_e$. Because the inverse reaction, $p + e^- \to n + \nu_e$, also proceeds, these two reactions tend to bring material in a chemical equilibrium. Thus, in the presence of many positrons produced by the pair creation, the fraction of protons and Y_e are increased (the neutron richness is reduced).

In the presence of an MNS that is a strong neutrino emitter, the neutrino irradiation to the matter surrounding the MNS can change its composition. Since neutrons and protons absorb neutrinos via $n + \nu_e \to p + e^-$ and $p + \bar{\nu}_e \to n + e^+$, respectively, the fractions of neutrons and protons tend to approach the values in a chemical equilibrium. Because the luminosity and average energy of ν_e and $\bar{\nu}_e$ from the MNS are not significantly different, p/n ratio changes from ~ 0.1 toward 1, and thus, Y_e also increases in the presence of the strong neutrino irradiation.

As already mentioned, there are two engines for the dynamical mass ejection: shock heating and tidal torque. For the MNS formation case, both effects play an important role. By the shock heating and neutrino irradiation from the MNS, Y_e for a large fraction of ejecta is significantly increased. On the other hand, matter ejected by the tidal torque does not efficiently undergo the weak interaction and the low-Y_e state is preserved. Therefore, the dynamical ejecta for the MNS formation case in general has components with a wide variety of Y_e between ~ 0.03 (i.e., the nearly original minimum value of NSs) and ~ 0.4 (cf. Fig. 4). If the effect by the weak interaction is subdominant, the fraction of low-Y_e ejecta is richer.

For the prompt BH formation case (high-mass NS-NS and BH-NS mergers), the dynamical mass ejection is induced primarily by the tidal effect. Thus, the ejecta tend to have low values of Y_e. In particular, for BH-NS mergers, the dynamical ejecta is dominated by the low-Y_e components with $Y_e < 0.1$ (cf. Fig. 6). This result is highly different from that

https://doi.org/10.1017/S1743921322001351 Published online by Cambridge University Press

in MNS-forming NS-NS mergers. For high-mass asymmetric NS-NS mergers leading to the prompt formation of a BH, the low-Y_e components are also dominant for the dynamical ejecta. However, because of the presence of the shock heating effect at the onset of the merger, a small fraction of the ejecta has high values of Y_e up to ~ 0.4.

3.2. *Post-merger mass ejection*

After many of NS mergers, an MNS or a BH surrounded by a disk is likely to be formed. Both the MNS and disk at their formation are differentially rotating and likely to be strongly magnetized, and hence, MHD turbulence could be induced. Then, strong turbulent viscosity could be enhanced as already mentioned in § 2. This viscous effect induces the so-called viscosity-driven post-merger mass ejection (Fernández & Metzger 2013; Metzger & Fernández 2014; Just et al. 2015; Fujibayashi et al. 2018).

Mechanism: The post-merger mass ejection is driven primarily from the disk orbiting the central compact object. We first summarize how this mass ejection proceeds. In the presence of the viscosity (which is supposed to be from the MHD turbulence), the disk is subject to long-term viscous heating and angular momentum transport. As indicated in Eq. (2.1) (replacing $R_{\rm inn}$ to a typical disk radius of 20–100 km), the timescale for this is several hundreds ms to a few seconds for the central objects of mass ~ 2–$10 M_\odot$. In an early stage of the disk evolution, for which the initial maximum density and temperature are $\gtrsim 10^{11}$ g/cm^3 and several MeV, thermal energy generated by the viscous heating is consumed primarily by the neutrino emission. In this stage, the disk expands by the angular momentum transport but the thermal energy generated cannot contribute a lot to the disk evolution. With the viscous expansion of the disk, its density and temperature decrease. By the decrease of the temperature, T, the neutrino emissivity is steeply reduced because it is approximately proportional to T^6 (e.g., Ruffert & Janka 1996). The latest numerical simulations have shown (e.g., Fujibayashi et al. (2020b)) that after the maximum temperature of the disk decreases below ~ 2–3 MeV, neutrino cooling timescale is longer than the viscous heating one. In this late stage, the viscous heating is fully used for the evolution of the (torus-shape) disk. Because the viscous heating is most efficient in the innermost region of the disk, convective motion is enhanced in the disk and activates efficiently carrying the thermal energy outward, in particular toward the torus surface. Primarily by this effect, the outer part of the disk (torus), which was already expanded by the viscous angular momentum transport, gains the thermal energy, and as a result, the matter in the outer region eventually escapes from the system as ejecta.

In the presence of strong magnetic fields, not only the viscous effects but also purely MHD effects play a role for the post-merger mass ejection (Siegel & Metzger 2017; Fernández et al. 2019; Christie et al. 2019; Shibata et al. 2021). However, the latest MHD simulations (Christie et al. 2019; Shibata et al. 2021; Hayashi et al. 2022) have shown that this is a subdominant effect for a reasonable magnetic-field profile. The neutrino-irradiation effect could also play a role for enhancing mass ejection in the presence of an MNS which is a strong neutrino emitter, but the latest simulation shows that this gives a subdominant effect for increasing the ejecta mass (Fujibayashi et al. 2020a), although the neutrino irradiation is one of the important effects for determining the electron fraction of the ejecta (see below).

Mass: Long-term (~ 10 s-long) numerical simulations have shown that the ejecta mass could be more than 30% of the initial disk mass, resulting in $M_{\rm eje,pm} = 0.05$–$0.1 M_\odot$, in the presence of a long-lived MNS (Metzger & Fernández 2014; Fujibayashi et al. 2018, 2020a). For the case that the MNS is the central object, the mass accretion onto it proceeds only after the thermal energy of the matter is dissipated by neutrino cooling. Because it takes neutrino-cooling timescale (~ 1 s) for this, which is comparable to the

https://doi.org/10.1017/S1743921322001351 Published online by Cambridge University Press

viscous timescale, the matter infall is suppressed, and consequently, the mass ejection is enhanced.

For the case that a BH is the central object, mass falling into it is appreciably larger than that of the outflow. However, numerical simulations for disks around spinning BHs show that 10–20% of the disk mass can be the ejecta component (e.g., Fernández & Metzger 2013; Just et al. 2015; Fujibayashi et al. 2020b,c; Just et al. 2021). MHD simulations show that in the presence of a strong poloidal magnetic field, the post-merger mass ejection is enhanced by the MHD process (Siegel & Metzger 2017; Fernández et al. 2019; Christie et al. 2019), but with initially toroidal-dominant magnetic field, which is likely to be more plausible, the enhancement of the mass ejection is not very significant (Christie et al. 2019; Shibata et al. 2021; Hayashi et al. 2022).

Velocity: The post-merger ejecta is launched primarily from the outer part of disks (tori). If the mass ejection takes place at a radius of $r \gtrsim 100Gc^{-2}M$ ($M = M_{\rm MNS}$ or $M_{\rm BH}$), the characteristic velocity would be $\lesssim 0.1c$. Hence, the typical velocity for the viscosity-driven ejecta component is smaller than that for dynamical ejecta. However, the velocity may be significantly enhanced in the presence of an MNS and dynamo action, because MHD turbulence could be developed enhancing the magnetic-field strength and forming global field lines around the MNS. After the development of the global magnetic field, the magneto-centrifugal effect (Blandford & Payne 1982) associated with the MNS rotation can play a significant role for the angular momentum transport and ejecta acceleration (Shibata et al. 2021). Also, as mentioned in § 2, the remnant MNS is differentially rotating, and thus, in the presence of turbulent viscosity, the angular momentum may be transported in the MNS with a short timescale (substitute $R_{\rm inn} \sim 10\,{\rm km} \sim H$ into Eq. (2.1)). Then, the angular-velocity profile of the MNS can be rearranged to be a nearly rigidly rotating one, and associated with the resulting rearrangement of the density and pressure profiles, strong pressure waves can propagate outward providing the energy to the matter in the outer region (Fujibayashi et al. 2018).

Irrespective of the MHD/viscous mechanisms described in the previous paragraph, the engine of the mass ejection is rotational kinetic energy in the presence of an MNS, which is estimated by $T_{\rm kin} \sim 0.3 M_{\rm MNS} R^2 \Omega^2$ (Cook et al. 1994), where $M_{\rm MNS}$, R, and Ω are the mass, equatorial radius, and angular velocity of the MNS, and thus,

$$T_{\rm kin} \sim 1.7 \times 10^{53} \left(\frac{M_{\rm MNS}}{2.6 M_\odot}\right) \left(\frac{R}{15\,{\rm km}}\right)^2 \left(\frac{\Omega}{7000\,{\rm rad/s}}\right)^2 {\rm erg}. \tag{3.1}$$

If $\sim 1\%$ of this energy is transferred to the ejecta, the average velocity of the ejecta evaluated by $\sqrt{2 \times 0.01 T_{\rm kin}/M_{\rm eje,pm}}$ is $\sim 0.15c (T_{\rm kin}/2 \times 10^{53}\,{\rm erg})^{1/2} (M_{\rm eje,pm}/0.1 M_\odot)^{-1/2}$ for the post-merger ejecta mass of $M_{\rm eje,pm}$. If the efficiency of the energy transfer is $\sim 10\%$, the average velocity of the ejecta could be $\sim 0.5c$. Hence, the typical velocity for the post-merger ejecta may be enhanced by a factor of ~ 2–3 in the presence of a long-lived MNS. However, the dynamo effect and subsequent magnetic-field growth are not well understood to date. One of the important topics in numerical relativity is to clarify these effects by a first-principle MHD simulations.

Electron fraction: The understanding of the electron fraction for the post-merger ejecta has been modified in the last three years, because long-term numerical simulations incorporating all the relevant physics such as weak interaction physics including neutrino effects and general relativity with more realistic initial conditions have been done in detail (e.g., Fujibayashi et al. 2018; Fujibayashi et al. 2020a; Fujibayashi et al. 2020b; Fujibayashi et al. 2020c; Just et al. 2021). What is important is that in the viscosity-driven post-merger mass ejection, the electron fraction is determined primarily by the long-term viscous evolution of the disk, and irrespective of the central object (MNS or BH), the electron fraction of the disk increases significantly during the viscous evolution.

https://doi.org/10.1017/S1743921322001351 Published online by Cambridge University Press

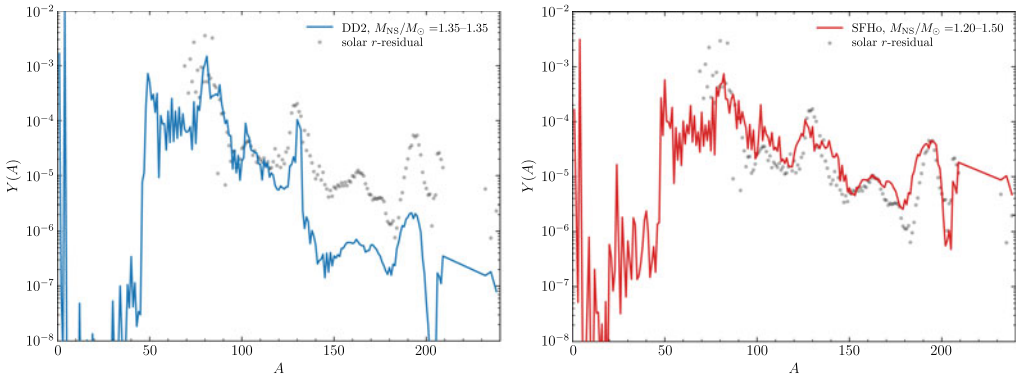

Figure 5. Elemental fraction for the r-process nucleosynthesis as a function of the mass number A for the models shown in Fig. 4. The small solid circles denote the solar-abundance. The solar abundance and numerical results are matched at $A = 90$. For the formation of a long-lived MNS (left), light r-process elements are overproduced (heavy elements are under-produced), and hence, the elemental pattern does not agree with the solar abundance pattern. By contrast, for the HMNS formation collapsing in ~ 20 ms after the onset of merger (right), the abundance pattern is in a good agreement with the solar abundance pattern.

As already mentioned, in its early stage, the density and temperature in the disk are high: The maximum density and temperature are $\gtrsim 10^{11}$ g/cm^3 and several MeV. In such conditions, the capture timescale of electrons and positrons by protons and neutrons and the timescale of the neutrino absorption by nucleons are shorter than the viscous timescale. That is, the following reactions are in equilibrium:

$$n + \nu_e \leftrightarrow p + e^-, \quad p + \bar{\nu}_e \leftrightarrow n + e^+, \tag{3.2}$$

and thus the chemical equilibrium $\mu_n + \mu_{\nu_e} = \mu_p + \mu_e$ is established (Beloborodov 2003). Here, μ_A $(A = n, p, \nu_e, e)$ denotes the chemical potential of each particle. By the viscous angular momentum transport, subsequently, the density and temperature of the disk decrease, and thus, neutrino absorption timescale becomes longer. However, the electron/positron capture timescales are still shorter than the viscous timescale for a while, and thus, the following reactions are still in equilibrium:

$$p + e^- \to n + \nu_e, \quad n + e^+ \to p + \bar{\nu}_e. \tag{3.3}$$

In the early stage of the disk evolution, the density is high, and thus, μ_e is dominant associated with the strong electron degeneracy, resulting in the neutron-rich (low-Y_e) state with $\mu_n \gg \mu_p$ (μ_{ν_e} is negligible in the disk). However, with the decrease of the disk density due to the viscous expansion, μ_e (which is approximately proportional to $\rho^{1/3}$) decreases, and as a result, the neutron richness becomes lower. Therefore, with the viscous evolution of the disk, the value of Y_e increases.

The post-merger mass ejection sets in when the neutrino cooling timescale becomes longer than the viscous timescale, at which the maximum temperature of the disk is ~ 2–3 MeV (Fujibayashi et al. 2020b; Just et al. 2021). Broadly speaking, below this temperature, all the timescales of the weak interaction becomes longer than the viscous timescale. Thus, approximately at the same time, the reactions of Eq. (3.3) freeze out and the electron fraction is fixed. Thus, the typical electron fraction of the post-merger ejecta is approximately determined by that at the moment of the freeze-out of the weak interaction (Fernández & Metzger 2013). The latest numerical simulations show that the typical value of Y_e at the freeze-out is ~ 0.2–0.4 irrespective of the central object (either MNS or BH) (Fujibayashi et al. 2020a,b,c; Just et al. 2021). In the presence of the MNS,

https://doi.org/10.1017/S1743921322001351 Published online by Cambridge University Press

Table 1. $M_{\rm ej,dyn}$ and $M_{\rm ej,vis}$: dynamical and post-merger ejecta mass in units of $M_\odot$, $Y_{e,\rm dyn}$: Y_e of dynamical ejecta, $Y_{e,\rm pm}$: Y_e of post-merger ejecta, $\langle v_{\rm ej,dyn}\rangle$: average velocity of dynamical ejecta in units of c. Low-m, Mid-m, and High-m imply that the remnants formed in ~ 1 ms after the merger are SMNS, HMNS, and BH.

Type of binary	Remnant	$M_{\rm ej,dyn}$	$M_{\rm ej,pm}$	$Y_{e,\rm dyn}$	$Y_{e,\rm pm}$	$\langle v_{\rm ej,dyn}\rangle/c$
Low-m NS-NS	SMNS	$O(10^{-3})$	0.05–0.1	0.03–0.4	0.2–0.5	0.15–0.20
Mid-m NS-NS (stiff EOS)	HMNS	$O(10^{-3})$	$O(10^{-2})$	0.03–0.4	0.2–0.5	0.15–0.25
Mid-m NS-NS (soft EOS)	HMNS	$\lesssim 10^{-2}$	$O(10^{-2})$	0.03–0.4	0.2–0.5	0.20–0.25
High-m NS-NS ($q\sim 1$)	BH	$< 10^{-3}$	$< 10^{-3}$	—	—	—
High-m NS-NS ($q < 1$)	BH	$O(10^{-3})$	$\lesssim 10^{-2}$	0.03–0.4	0.2–0.5	0.2–0.3
BH-NS	BH	0–0.1	0–0.1	0.03–0.1	0.1–0.4	0.2–0.3

which is the strong neutrino emitter, the electron fraction of the ejecta could be even higher due to the neutrino irradiation (Metzger & Fernández 2014; Fujibayashi et al. 2018), but this effect is subdominant. The actual electron fraction is widely distributed as in dynamical ejecta. However, the low end is at smallest ~ 0.2 for the viscous hydrodynamics with plausible viscous parameters. In the MHD simulations, the lower end can be smaller, up to ~ 0.15, because the purely MHD effects can eject matter within the viscous timescale. On the other hand, the high end is always $\gtrsim 0.5$.

The typical property of ejecta is summarized in Table 1, which shows that the ejecta property depends strongly on the binary parameters. In Fig. 4, we also show numerical results for the mass histogram as a function of Y_e for the formation of a long-lived MNS (left) and a HMNS that collapses into a BH at ~ 20 ms after the onset of merger (right). The dotted and solid curves denote the contributions from dynamical and post-merger ejecta, respectively, each of which results from the merger and subsequent post-merger simulations (Fujibayashi et al. 2022). It is found that the ratio of the masses of the dynamical ejecta to the post-merger ejecta is larger for the HMNS formation case while it is small (of $O(10^{-2})$) for the long-lived MNS formation case, as summarized in Table 1. The main reason is that for the formation of the long-lived MNS, the mass of the post-merger mass ejection becomes very large.

Figure 5 shows the results of a nucleosynthesis calculation for the models presented in Fig. 4 (Fujibayashi et al. 2022). For the long-lived MNS formation, a large amount of the light r-process elements with $A \lesssim 100$ are synthesized primarily from the post-merger ejecta while the amount of the heavy r-process elements ($A \gtrsim 130$) synthesized from the dynamical ejecta is quite small. For this case, the abundance pattern is significantly different from the solar abundance pattern. By contrast, for the formation of the HMNS with a short lifetime of $O(10)$ ms, the abundance pattern is close to the solar abundance pattern. Suppose that the NS mergers would be the major site for the r-process nucleosynthesis and the abundance pattern of the r-process elements would be universally similar to the solar pattern in the universe. Then, the frequent formation of the long-lived MNS in the NS mergers is disfavored, while the frequent formation of the short-lived HMNS is favored. Otherwise, the solar abundance pattern of the r-process elements cannot be reproduced.

A word of caution is appropriate here. To derive the quantitative results for the properties of the post-merger ejecta, self-consistent long-term simulations have been performed for the MNS formation (Fujibayashi et al. 2018, 2020a, 2022). However, for the case of prompt BH formation, the post-merger simulations have been performed starting from ad hoc initial conditions for the matter profile of disks and magnetic-field configurations or for the hypothetical viscous coefficient (e.g., Fernández & Metzger 2013; Just et al. 2015; Siegel & Metzger 2017; Christie et al. 2019; Fujibayashi et al. 2020b,c; Just et al. 2021). Thus, the results can depend significantly on the initial condition employed, and in the viscous-hydrodynamics simulations, they can depend on the viscous parameter.

https://doi.org/10.1017/S1743921322001351 Published online by Cambridge University Press

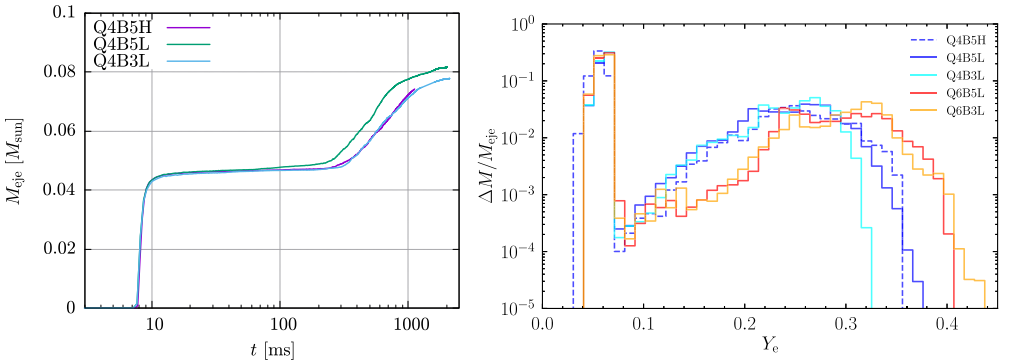

Figure 6. Left: Mass ejection history for BH-NS merger models with the BH mass of $5.4M_\odot$, BH dimensionless spin of 0.75, and NS mass of $1.35M_\odot$. Right: Mass histogram as a function of Y_e for the ejecta of BH-NS mergers. Q4 and Q6 denote the models with the BH mass of $5.4M_\odot$ and $8.1M_\odot$. See Hayashi et al. (2022) for more details.

To overcome these problems, we need to perform a long-term simulation from the merger to the post-merger stages self-consistently. The topic of the next section is on our latest effort to this direction.

4. First self-consistent simulation

As we described above, we need a long-term simulation which can fully explore the process from the merger up through the post-merger mass ejection stage, to establish a self-consistent picture for the entire mass ejection and resultant r-process nucleosynthesis. We have recently performed seconds-long simulations for BH-NS binaries for the first time (Hayashi et al. 2022). This section is devoted to briefly introducing the results of this work.

We performed a neutrino-radiation MHD simulation in full general relativity for the merger between BHs and an NS. The BH mass is $5.4M_\odot$ or $8.1M_\odot$ with the dimensionless spin of 0.75. The NS mass is $1.35M_\odot$ with a relatively stiff equation of state that gives the NS radius of 13.2 km. In this setting, the NS is tidally disrupted before it is swallowed into the BH, and at the merger, the matter with mass of 0.04–$0.05M_\odot$ is dynamically ejected in the first ~ 10 ms (see the left panel of Fig. 6) and a disk with the initial mass of 0.2–$0.3M_\odot$ is formed (for lower initial BH mass, the value is larger). The disk is subsequently evolved by the MHD effects. As described in § 2 and § 3, the MHD turbulence is developed primarily by the MRI and winding in the disk, and subsequently, effective viscosity is induced and drives the post-merger mass ejection. The post-merger mass ejection sets in at ≈ 0.3–0.5 s after the tidal disruption at which the neutrino luminosity becomes sufficiently low (see the left panel of Fig. 6 for the mass ejection history). The resulting post-merger ejecta mass is 0.02–$0.03M_\odot$ (i.e., about 10% of the initial disk mass). All these results for the post-merger mass ejection are in fair agreement with those for the latest long-term simulations to BH-disk systems in general relativity (e.g., Fujibayashi et al. 2020b,c).

The right panel of Fig. 6 shows the mass histogram of the ejecta as a function of Y_e for several models of BH-NS mergers with different BH mass and different initial magnetic-field strength. It is found that irrespective of the setting, two components emerge; one is the dynamical ejecta with $Y_e < 0.1$ and the other is the post-merger ejecta with $Y_e \approx 0.1$–0.4. The two-components distribution of Y_e agrees semi-quantitatively with that described in § 3. The values of Y_e are slightly smaller than those predicted by viscous

https://doi.org/10.1017/S1743921322001351 Published online by Cambridge University Press

hydrodynamics simulations (Fujibayashi et al. 2020b; Just et al. 2021). Our interpretation for this is that by the purely MHD effect, the matter in the inner region of disk, which has relatively low values of Y_e, can be ejected. However, besides this minor quantitative difference, the mass histogram of the post-merger ejecta is similar to that found in the post-merger simulations.

The seconds-long MHD simulation exploring both for the merger and post-merger stages is obviously suitable for fully understanding the mass ejection mechanisms. In the next decade, we need to focus on our effort along this line.

References

Abbott, R. et al. 2021, *arXiv: 2111.03606*
Abbott B.P. et al. 2017, *Phys. Rev. Lett.*, 119, 161101
Abbott B. et al. 2020, *Astrophys. J. Lett.*, 892, L3
Balbus, S.A. & Hawley, J.F. 1998, *Rev. Mod. Phys.*, 70, 1
Barnes, J. & Kasen, D. 2013 *Astrophys. J.* 775, 18
Beloborodov, A.M. 2003 *Astrophys. J.* 588, 931
Blandford, R.D. & Znajek, R.L. 1977, *Mon. Not. R. Astron. Soc.* 179, 433
Blandford, R. & Payne, D.G. 1982, *Mon. Not. R. Astron. Soc.* 199, 883
Christie, I.M., et al. 2019, *Mon. Not. R. Astron. Soc.* 490, 4811
Cook, G.B., Shapiro, S.L., & Teukolsky, S.A. 1994, *Astrophys. J.* 423, 823
Fernández, R. & Metzger, B.D. 2013, *Mon. Not. Royal Astron. Soc.* 435, 502
Fernández, R., Tchekhovskoy, A., Quataert, E., Foucart, F., & Kasen, D. 2019,*Mon. Not. R. Astron. Soc.* 482, 3373
Fujibayashi, S., et al. 2018, *Astrophys. J.* 860, 64
Fujibayashi, S., et al. 2020, *Astrophys. J.* 901, 122
Fujibayashi, S., et al. 2020, *Phys. Rev. D* 101, 083029
Fujibayashi, S., et al. 2020, *Phys. Rev. D* 102, 123014
Fujibayashi, S., et al. 2022, in preparation
Hayashi, K. et al. 2022 *Phys. Rev. D* in submission (arXiv: 2111.04621)
Hotokezaka, K, Kiuchi, K, Kyutoku, K., Okawa, H., Sekiguchi, Y., Shibata, M. & Taniguchi, K. 2013, *Phys. Rev. D* 87, 024001
Just, O., Bauswein, A., Pulpillo, R.A., Goriely, S., & Janka, H.-Th. *Mon. Not. Royal Astron. Soc.* 448, 541
Just, O. et al. 2021, *ArXiv: 2102.08387*
Kiuchi, K. et al. 2014, *Phys. Rev. D* 90, 041502
Kyutoku, K. et al. 2021, *Living Review Relativity* 24, 5
Metzger, B.D. & Fernández, R. 2014, *Mon. Not. Royal. Astron. Soc.* 441, 3444
Nedora, V. et al. 2021, *Astrophys. J.* 906, 98
Price, D.J., & Rosswog, S. 2006, *Science* 312, 719
Radice, D. et al. 2018, *Astrophys. J.* 869, 130
Ruffert, M. & Janka, H.-Th 1996, *Astron. Astrophys.* 344, 573
Shibata, M 2016 *Numerical Relativity (World Scientific, Singapore)*
Shibata, M., Fujibayashi, S., Hotokezaka, K., Kiuchi, K., Kyutoku, K., Sekiguchi, Y. & Tanaka, M. 2017, *Phys. Rev. D* 96, 123012
Shibata, M., & Hotokezaka, K. 2019, *Ann. Rev. Nucl. Part. Sci.*, 69, 41
Shibata, M. et al. 2021, *Phys. Rev. D* 104, 063026
Siegel, D.M. & Metzger, B.D. 2017, *Phys. Rev. Lett.* 119, 231102
Tanaka, M. & Hotokezaka, K. 2013, *Astrophys. J.* 775, 113

https://doi.org/10.1017/S1743921322001351 Published online by Cambridge University Press